J Geod (2016) 90:189–203
DOI 10.1007/s00190-015-0865-6

ORIGINAL ARTICLE

Ionospheric corrections for single-frequency tracking of GNSS satellites by VLBI based on co-located GNSS

Benjamin Männel[1] · **Markus Rothacher**[1]

Received: 15 April 2015 / Accepted: 13 October 2015 / Published online: 27 October 2015

Abstract Tracking L-band signals of GNSS satellites by radio telescopes became a new observation type in recent years and will be used to improve reference system realizations and links between Earth- and space-fixed frames. First successful test observations were done, with the drawback of being single-frequency only. In order to correct the ionospheric delay by using GNSS phase observations from co-located receivers, the L4R approach was developed. Based on residuals derived by a least-squares processing of the GNSS geometry-free linear combination corresponding corrections could be derived. As a first validation step L4R corrections were applied to GNSS L_1 data analysis. Station coordinate repeatibilities at the 1-cm level were obtained for baselines of a few thousand kilometers. Comparing the derived delay corrections to VLBI ionospheric delays for quasars located in same directions, differences with a standard deviation of 2.2 TECU could be achieved.

Keywords VLBI · GNSS · Co-location in space · Ionospheric delay · Geometry-free linear combination · VLBI satellite-tracking

1 Introduction

1.1 Tracking satellites by radio telescopes

In recent years co-location in space, combining Global Navigation Satellite Systems (GNSS), Satellite Laser Ranging (SLR) and Doppler Orbitography and Radiopositioning Integrated by Satellite (DORIS) on-board existing low earth orbiters (LEOs) and GNSS satellites, was used as an alternative to the combination of these techniques at ground stations (Thaller et al. 2011; Flohrer et al. 2011). Due to missing X/S-band transmitters on-board satellites, suited for co-location in space, and due to the fact that geodetic used radio telescopes are mainly not sensitive to the signals typically emitted by satellites, so far Very Long Baseline Interferometry (VLBI) was excluded from co-location in space. Considering the advantages of including VLBI into the combination of space geodetic techniques in space for determining the International Terrestrial Reference Frame (ITRF) and realizing the connection to the International Celestial Reference Frame (ICRF) in space, two scenarios are foreseeable. On the one hand suitable X/S-band transmitters will be brought into orbit by future satellite missions dedicated to co-location in space like GRASP (Bar-Sever et al. 2009). This will take some years from today. On the other hand, in recent years a few geodeticly used radio telescopes tracked the L-band signals of GNSS satellites. Observing GPS by radio telescopes was proposed by Hase (1999) and further discussed among others by the working group on GPS Phase Center Mapping (Corey 2001), by Dickey (2010) and by Plank et al. (2014). The first baseline tracking GLONASS L_1 signals (1.598–1.605 GHz) was realized in 2010 by the 32 m radio telescopes at Medicina and the 25 m telescope at Onsala usually used for astrometry (Tornatore et al. 2011, 2014). According to Haas et al. (2014), a stochastic measurement noise of 4 ps in 15 min could be achieved. In 2013, using the 25 m telescope at Onsala and the S-Band horn and a special L-Band receiver at the 20 m radio telescope at Wettzell (RTW) a second baseline was observing GLONASS L_1 signals (Kodet et al. 2014); the RMS-scatter of the derived phase delays was below 10 ps in 2 s (Haas et al. 2014). These single-frequency observations are the best G-VLBI measurements currently available, therefore, corrections for the ionosphere are essential.

✉ Benjamin Männel
maennelb@ethz.ch

[1] ETH Zurich, Zurich, Switzerland

In general, two observation strategies are feasible: (1) alternate observations to a GNSS satellite and to calibrator sources (namely quasars), and (2) stand-alone observations to a GNSS satellite. The first concept is known as phase-referencing or D-VLBI in deep space navigation for many years. Plank (2013) gives an overview concerning the applications of D-VLBI for near-Earth and lunar missions. Within this paper a tracking based on the second concept was assumed, as it was used for the Onsala–Wettzell experiments described above. To distinguish between both strategies this concept will be called "G-VLBI". Due to bandwidth limitations of the feed horns and receivers, the L_2 signal with a lower frequency was not tracked so far, and at least for a number of radio telescopes, participating regularly in IVS sessions, L_2 cannot be tracked because of that limitation. For single-frequency observations the ionospheric refraction will become the major error source. Within this paper a method to estimate ionospheric delays using co-located GNSS receivers is presented (named L4R approach). The impact of the ionosphere on radio frequency waves will be introduced in the next subsection. The estimation of ionospheric delays and corrections will be described in Sect. 2. Also the error budget as well as advantages and disadvantages compared to other methods will be discussed. Corresponding results will be presented in Sect. 3 and two validation steps and results thereof will be discussed in Sects. 4 and 5. Conclusions and outlook follow in Sect. 6.

1.2 Ionospheric impact on microwave observations in space geodesy

Traveling through the upper atmosphere, the so-called ionosphere (50–1000 km above Earth's surface), microwave signals (0.3…300 GHz) are disturbed by free electrons. The disturbance of the signal phase can be expressed by the phase refractive index n_{ph}:

$$n_{\mathrm{ph}} = 1 - a\frac{N_{\mathrm{e}}}{f^2} \text{ with } a = 40.3 \cdot 10^{16}\left[\frac{\mathrm{m}^3}{\mathrm{s}^2 \cdot \mathrm{TECU}}\right] \quad (1)$$

with the electron density N_{e} and the signal frequency f. Using the total electron content (TEC) E

$$E = \int N_{\mathrm{e}}(s)\mathrm{d}s, \quad (2)$$

expressed in total electron content units per square meter (TECU), along the signal path s, the ionospheric delay I_{c} for code and the advance I_{ph} for phase measurements can be written as follows:

$$I_{\mathrm{c/ph}} = \pm\frac{aE}{f^2}. \quad (3)$$

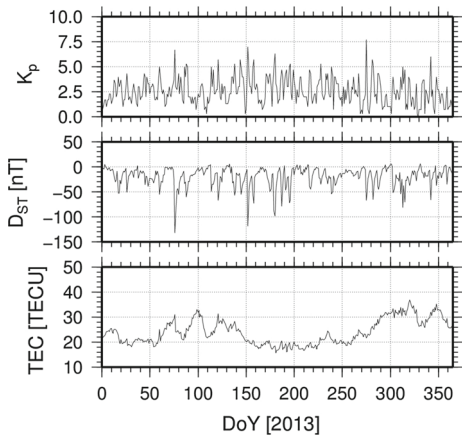

Fig. 1 Ionospheric characterization 2013. *Top* daily maximum K_P index, *middle* daily minimum D_{ST} index and *bottom* daily mean TEC (from CODE GIMs)

During ionospheric storms this density will be highly perturbed (Prölss 2008). Figure 1 shows the ionospheric behavior during 2013 based on three different quantities. The first quantity, the 3 h K_p index,[1] characterizes the effect of solar particles on the Earth's magnetic field in 27 steps from 0 to 9. An ionospheric storm is typically indicated by values above 5. In Fig. 1 the daily maximum values are shown, exceeding 5 only for a few days. The second quantity, the disturbed storm time index[2] D_{ST} represents the strength of the ring current around the Earth caused by solar particles. As the ring current is directed opposite to Earth's magnetic field, negative values indicate a weakening. Therefore, the daily minimum value is plotted. Values below −100 nT, indicating a moderate/strong ionospheric storm, occur only twice. The third quantity, the daily global mean TEC derived from GNSS observations, represents the seasonal variability of the electron density. For each day the degree 0 and order 0 coefficient between 12 UT and 14 UT given in the global ionospheric maps (GIM) provided by the Center of Orbit Determination in Europe (CODE) (Schaer 1999) is plotted. Concerning solar activity, 2013 is part of the very weak solar cycle 24.

The relationship between delay and frequency allows to minimize the ionospheric delay using dual-frequency measurements and the ionosphere-free linear combination thereof. Using X- and S-band signals in VLBI the remaining ionospheric delay is negligible (Hawarey et al. 2005), for GNSS so-called second- and third-order terms have to be considered (Fritsche et al. 2005). If only single-frequency observations are available the delay for X-band VLBI observations will be, depending on the elevation, between 0.1 and

[1] http://umbra.nascom.nasa.gov/sdb/yohkoh/ys_dbase/indices_raw/2013, Oct 2014.

[2] http://www.wdcb.ru/stp/data/geomagni.ind/dst/dst2013.txt, Oct 2014.

2 ns, corresponding to 4…60 cm (Sovers et al. 1998). For GNSS L-band signals the delay will be between 3 and 15 ns (1…15 m). Derived baseline lengths will be shortened by a scaling factor of about 1 ppm per 10 TECU (Beutler et al. 1988) assuming a cut-off angle of 15°. Considering G-VLBI as described in Sect. 1.1, i.e. for co-location in space, correcting the ionospheric delay will be mandatory (Männel et al. 2014). In the following section we present an approach suited for deriving ionospheric corrections in the case of G-VLBI observations.

2 The L4R approach

2.1 Idea and formalism

As G-VLBI will observe GNSS L-band signals, the ionospheric delay between a GNSS satellite i and a radio telescope will almost be identical to the delay between the GNSS satellite i and a co-located GNSS receiver r, located not more than a few hundred meters apart. Therefore, an ionospheric delay between satellite i and GNSS receiver r determined by dual-frequency GNSS observations can be used to correct the ionospheric delay in the G-VLBI observation (Fig. 2). In principle, the ionospheric delay for a special satellite-baseline pair could be estimated using GNSS code observations on the single-difference level as described by Hernández-Pajares et al. (2011). The accuracy of the derived delays will be at several TECU (corresponding to a few meters in L_1) due to measurement noise, multipath effects and uncertainties in the differential code biases. Using the phase observations L_1 and L_2, ionospheric delays can be computed with the geometry-free linear combination $L_4 = L_1 - L_2$, where the geometrical range and all frequency-independent biases are removed. In order to get rid of phase biases and resolve the carrier phase ambiguities, double differences are formed. For a combined GPS/GLONASS double-difference analysis the geometry-free linear combination can be written in metric units as follows:

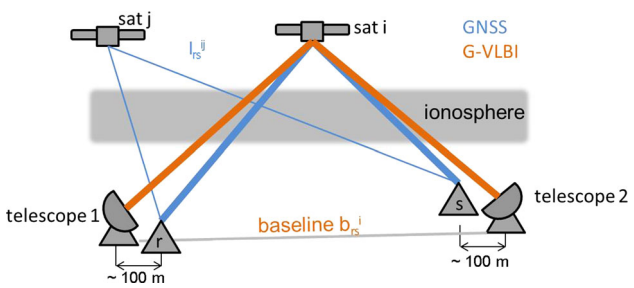

Fig. 2 The idea of L4R, the signal paths of GNSS and G-VLBI within the ionosphere can be assumed as identical

$$
\begin{aligned}
L^{ij}_{rs,4} &= L^{ij}_{rs,1} - L^{ij}_{rs,2} \\
&= \lambda^i_1 \Phi^i_{rs,1} - \lambda^i_2 \Phi^i_{rs,2} - \lambda^j_1 \Phi^j_{rs,1} + \lambda^j_2 \Phi^j_{rs,2} \\
&\quad + \Delta\lambda^{ij}_1 N^j_{rs,1} - \Delta\lambda^{ij}_2 N^j_{rs,2} - \lambda^i_1 N^{ij}_{rs,1} + \lambda^i_2 N^{ij}_{rs,2} \\
&\quad - \frac{f_1^2 - f_2^2}{f_1^2 f_2^2} I^{ij}_{rs} + \epsilon^{ij}_{rs,4}.
\end{aligned}
$$

Here $\Phi^i_{rs,n}$ is the phase observation in cycles between receivers r and s and the satellite i at frequency L_n, $n = (1, 2)$.

The corresponding signal wavelength is given by λ_i and the difference between the wavelengths of different satellites is $\Delta\lambda^{ij}_n$. These differences are only relevant for GLONASS, where satellites have different carrier frequencies. As a consequence also the single-differenced ambiguities $N^j_{rs,n}$ for the reference satellite j are part of the observation equation. The small biases present in $L^{ij}_{rs,4}$ due to the frequency difference between the two GLONASS satellites are not significant as $\Delta\lambda^{ij}_n$ will not exceed 1.5 mm for L_1 and 2.0 mm for L_2. However, the term $\Delta\lambda^{ij}_1 N^j_{rs,n}$ will cause problems when fixing the ambiguities. Noise and multipath effects are absorbed in $\epsilon^{ij}_{rs,4}$. After fixing the ambiguities $N^{ij}_{rs,n}$ for GPS and GLONASS only the ionospheric delay I^{ij}_{rs} contained in L_4 remains in the residuals (i.e. observed-computed) $\hat{I}^{ij}_{rs}$ computed during a least-squares adjustment. As an alternative to fixing ambiguities, phase observations can be leveled to the corresponding code pseudoranges. But the disadvantages mentioned in the first paragraph of this section—except for the noise level—remain and, therefore, we did not pursue this strategy. It should be mentioned, however, that considerable progress was made lately in the determination of the zero-difference code biases in the context of zero-difference ambiguity resolution.

To apply double-difference ionospheric delay corrections to G-VLBI observations, first single-difference residuals have to be derived from the double-difference residuals. Because $n - 1$ linearly independent double-differences have to be transformed into n single-differences $\hat{I}^i_{rs}$, an additional and independent constraint has to be applied. Following Alber et al. (2000) by introducing a weighted zero-mean condition $\sum_x \omega^x_{rs} \hat{I}^x_{rs} = 0$ with the weights ω^x_{rs}, this regularization step can be written as follows:

$$
\begin{bmatrix}
1 & -1 & 0 & 0 & 0 \\
1 & 0 & -1 & 0 & 0 \\
\vdots & \vdots & \ddots & \ddots & \vdots \\
\vdots & \vdots & \ddots & \ddots & \vdots \\
\omega^1_{rs} & \omega^2_{rs} & \dots & \dots & \omega^n_{rs}
\end{bmatrix}
\cdot
\begin{bmatrix}
\hat{I}^1_{rs} \\ \hat{I}^2_{rs} \\ \vdots \\ \hat{I}^n_{rs}
\end{bmatrix}
=
\begin{bmatrix}
\hat{I}^{11}_{rs} \\ \hat{I}^{12}_{rs} \\ \vdots \\ \hat{I}^{1n}_{rs} \\ \sum_{x=i1}^{in} \omega^x_{rs} \hat{I}^x_{rs}
\end{bmatrix}. \qquad (4)
$$

As indicated by the indices $\hat{I}^x_{rs}$, Eq. 4 has to be computed baseline-wise using the observations to all common satellites. The zero-mean condition has to be introduced for each measurement epoch. A weighting function has not been applied in our case. Once the single-difference residuals have been computed, they represent the difference of the ionospheric delays between the two stations, or in other words, the relative ionospheric delays. The absolute part of the ionospheric delay $\overline{I}_{rs}$ cannot be computed by this approach and is applied using an ionospheric model, i.e. the GIMs produced by CODE in our case. The corresponding equation for the total ionospheric delay correction I^i_{rs} can be written as follows:

$$I^i_{rs} = \hat{I}^i_{rs} + \overline{I}_{rs}. \tag{5}$$

The model part is defined by

$$\overline{I}_{rs} = \frac{\sum_{x=1}^{n} I^x_{rs}}{n} = \frac{\sum_{x=1}^{n} (I^x_r - I^x_s)}{n}, \tag{6}$$

where n is the number of observed satellites (i.e. the number of single-differences) and I^i is the satellite-specific ionospheric correction derived from the model. In the following this algorithm will be called L4R.

2.2 Extension to zero-difference residuals

In principle the described regularization step can be applied for a second time to derive zero-difference delays, i.e. delays for individual satellite-receiver pairs. In analogy to Eq. 4 this step can be written as follows:

$$\begin{bmatrix} 1 & -1 & 0 & 0 & 0 \\ 1 & 0 & -1 & 0 & 0 \\ \vdots & \vdots & \ddots & \ddots & \vdots \\ \vdots & \vdots & \ddots & \ddots & \vdots \\ \omega^i_1 & \omega^i_2 & \dots & \dots & \omega^i_n \end{bmatrix} \cdot \begin{bmatrix} \hat{I}^i_1 \\ \hat{I}^i_2 \\ \vdots \\ \hat{I}^i_n \end{bmatrix} = \begin{bmatrix} \hat{I}^i_{12} \\ \hat{I}^i_{13} \\ \vdots \\ \hat{I}^i_{1n} \\ \sum_{x=12}^{1n} \omega^i_x \hat{I}^i_x \end{bmatrix} \tag{7}$$

As indicated by the index $\hat{I}^i_x$, all observations to one satellite are processed together; therefore, only linearly independent baselines should be introduced. The total ionospheric delay corrections I^i_r is then

$$I^i_r = \hat{I}^i_r + \overline{I}_r \quad \text{with } \overline{I}_r = \frac{\sum_{i=1}^{n} I^n_r}{n}. \tag{8}$$

2.3 Implementation

An adapted version of the Bernese GNSS Software V5.2 (Dach 2013) was used for this work. Additional subroutines were implemented to read and process VLBI observations to satellites and quasars (based on the work of Schmid 2009) and to transform double-difference residuals into baseline-wise residuals (based on the work of Wang et al. 2014). Also the splitting into zero-difference residuals and the possibility to introduce ionospheric corrections into GNSS and G-VLBI observations were implemented. In Fig. 3 the processing procedure is shown. Following the GNSS part, where ambiguities are resolved, the L_4 residuals are computed and the regularization (based on Eq. 4) is performed. Then the estimated ionospheric corrections are introduced into the G-VLBI processing. The validation steps in Fig. 3 will be described in Sects. 4 and 5. The processing of daily sessions is automated using the Bernese Processing Engine (BPE).

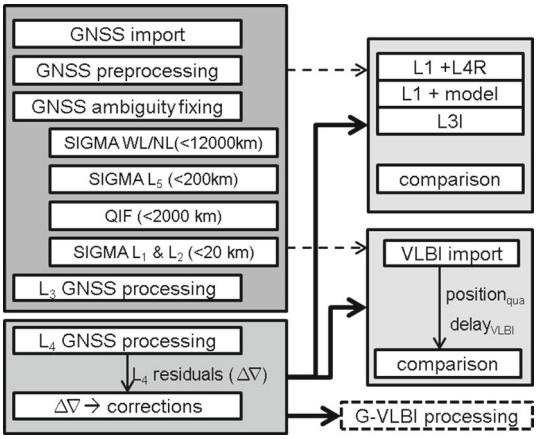

Fig. 3 Processing procedure, the *upper left box* is a common GPS/GLONASS processing, *lower left* the L4R processing, *upper right* validation 1, *middle right* validation 2 and *lower right* the intended correction of G-VLBI observations

2.4 Accuracy level and remaining error sources

Plank (2013) showed weekly station coordinate repeatabilities of 5–10 mm based on 800–1300 simulated G-VLBI observations per day. Assuming an error of the ionospheric delay correction for an individual observation below 2 TECU (corresponding to 32 cm in L_1 and 20 ps in X-band), these coordinate repeatabilities could be reached. In the following these values will be used during the validation using external solutions. A value of 0.3 TECU (5 cm in L_1) will be used when analyzing the scatter of the L4R-derived ionospheric corrections.

Apart from the ionospheric signal the residuals $L^{ij}_{rs,4}$ will contain errors related to unresolved ambiguities and non-ionospheric, station-specific biases like multipath effects and receiver noise. These non-ionospheric biases are mainly elevation-dependent and can reach cm-level for very short baselines (below 100 m) as shown by Wang et al. (2014). Considering baseline lengths that are typical for VLBI (hundreds to thousands of km) these biases are negligible (Crocetto et al. 2008).

Remaining unresolved ambiguities in the least squares adjustment will be estimated as real numbers and will, therefore, influence the corresponding residuals by partly absorbing the ionospheric signal. Using the possibilities of the Bernese GNSS Software, a considerable effort is made to fix as many ambiguities as possible. The corresponding ambiguity resolution process is similar to the one described in Steigenberger et al. (2006). In a first step, widelane ambiguities are fixed using the Melbourne-Wübbena linear combination. In a second step, this is done using phase observations only. Due to ionospheric delays processing phase observations by this method is only reasonable for baselines shorter than 200 km. The quasi-ionospheric free (QIF) algorithm is the next step that is applied to baselines up to 2000 km and followed by the SIGMA algorithm applied directly to the L_1 and L_2 phase data. For GLONASS ambiguities only the SIGMA algorithm for phase data is usable (Dach et al. 2007). To evaluate the impact of absorbing ionospheric delays into float ambiguities as a worst-case scenario, a float solution was computed and compared to the residuals of a solution including ambiguity fixing. For the float solution residuals are smaller by up to 20 cm (approx. 1 TECU) for baselines of around 1000 km and up to 50 cm (approx. 3 TECU) for baselines longer than 5000 km.

A third error source arises by introducing absolute delays derived from a (smoothed) model. The CODE GIMs used are developed into spherical harmonics of degree and order 15 valid for two hours. The accuracy of such GIMs is, according to Hernández-Pajares et al. (2011), between a few and 10 TECU in the vertical component depending on solar cycle, station latitude, station local time and geomagnetic activity.

2.5 Comparison with other methods

Naturally, since the ionospheric delays are varying fast in space and time, the quality of a correction approach depends on the deriving of the corrections as closely as possible in time, location and direction to the actual observations. Therefore, the different methods are compared with respect to their proximity to the observing situation (including usage of same equipment) and their limitations regarding secondary or technique-specific error sources. Also the applicability of a correction has to be considered (i.e. the range of possible applications, the effect on the observation scenario and additional processing load). In Table 1 we compare the following approaches to correct ionospheric delays for single-frequency satellite tracking: (1) introduction of TEC maps resp. GIMs (e.g. Sekido et al. 2003; Gordon 2010;

Table 1 Comparison of diverse approaches to derive ionospheric corrections for VLBI processing

	TEC maps	Local VTEC	D-VLBI[a]	L4R
Corrections based on				
GNSS	X[b]	X		X
VLBI			X	
Same source				X
Same telescope(s)			X	
Same frequency			X	X
Same signal path			X[c]	X[d]
Same epoch		X	X	X
Limitations				
Quality GNSS proc.	X	X		X
Plasma effects[e]			X	
Mapping function	X	X		
Temporal smoothing	X			
Spatial smoothing	X	X		
Co-located GNSS rec.		X		X
Add. quasar obs.			X	
Additional processing		X		X
Applications				
Single-freq. VLBI	X	X		
G-VLBI	X	X	X	X
Planetary S/C	X	X	X	

[a] Also known as phase-referencing, only the same beam method is considered (Kikuchi et al. 2008)
[b] TEC maps based on other techniques (e.g. ionograms) are not considered here
[c] Assuming a 1° separation the signal paths are separated by roughly 7 km at a height of 400 km
[d] Assuming a local tie of 100 m the signal paths are separated by 98 m at a height of 400 km
[e] Interplanetary and interstellar plasma

Tierno Ros et al. 2011), (2) estimating the local vertical TEC (VTEC) (Sardon et al. 1994), (3) using D-VLBI (e.g. Duev et al. 2012; Kikuchi et al. 2009) and (4) using L4R.

From Table 1 one can conclude that TEC maps are easy to apply but limited temporal and spatial resolution reduces the quality of derived corrections (Gordon 2010; Tierno Ros et al. 2011). TEC maps are also an input for some of the other methods, like L4R or phase-referencing. Local VTEC values derived from co-located GNSS observations might by a good option; however, errors are introduced by mapping the vertical TEC to the observation direction. Compared to both, the methods D-VLBI and L4R are superior, as the actual ionospheric situation in observation direction is taken into account. Both methods are using an additional observation closely aligned to the observed signal path. As the ionosphere also varies with the direction (expressed by ionospheric gradients) the separation angle between both signals has to be small. In L4R the maximal separation is given by the distance between radio telescope and GNSS receiver, which is usually below 1 km. In the case of GNSS satellites the choice of the maximal separation angle in D-VLBI is a delicate trade-off between baseline length, the number of calibrator sources and the variability of the ionosphere. Based on that Plank (2013) concludes that a modified D-VLBI concept might be necessary to track GNSS satellites. However, using a large set of calibrator sources, D-VLBI might be applicable to derive ionospheric corrections. In summary, we conclude that the L4R method to derive ionospheric corrections for single-frequency tracking of GNSS satellite is currently the most promising approach.

3 Ionospheric results derived by L4R

Within this section the ionospheric delays derived by the L4R approach will be discussed in three main parts. After a short introduction of the used database, first, the differences between double-difference residuals and corresponding CODE GIM values allow to characterize the processing results. Second, the splitting of double-difference into single-difference residuals will be studied to assess the impact of the introduced zero-mean condition. And third, the station-specific ionospheric behavior will be discussed using zero-difference residuals. All result are given for the GNSS L_1 frequency.

3.1 Database

For the following work 11 fundamental sites in Europe and North America (Fig. 4), each equipped with a radio telescope contributing to the International VLBI Service for Geodesy and Astrometry (IVS), were used to analyze potential G-VLBI baselines. The selected stations allow to compare (1) different baseline lengths and (2) different baseline orientations. All selected sites are also equipped with at least one co-located GPS or even GNSS receiver participating in the International GNSS Service (IGS). Table 2 gives an overview of the selected sites including the distances between radio telescope and GNSS receiver as given by the ITRF2008 (Altamini et al. 2011). GNSS observations with a data rate of 30 s, provided as RINEX files, were used to derive the ionospheric delays. For validation also VLBI observations given in NGS card file format provided by the IVS were used. More details will be given in Sect. 5.1. Final GNSS orbits and 30 s clocks, as well as Earth rotation parameters and ionospheric maps provided by CODE and coefficients for the VMF tropospheric mapping function provided by TU Vienna (Böhm et al. 2006) were used. During the analyzed period (2013, Jan 1 to Dec 31) only minor data gaps occurred, e.g. RINEX files for day of year (DoY) 265–294 are missing for station WES2.

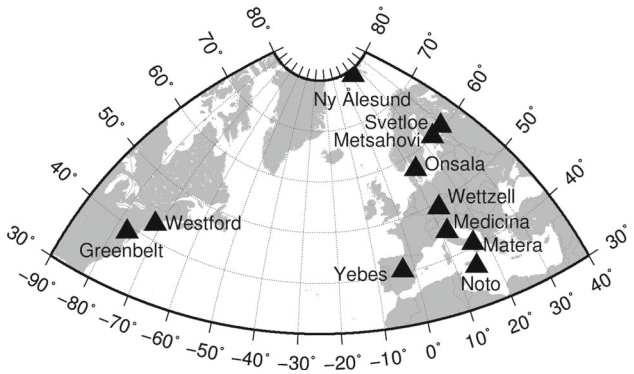

Fig. 4 Map of fundamental sites, the station names according to IGS and IVS are given in Table 2

Table 2 Selected radio telescopes and GNSS receivers for each fundamental site; sys indicates available GNSS systems; G = GPS, R = GLONASS; distance between VLBI and GNSS

Site	VLBI telescope	GNSS		Distance (m)
		Receiver	Sys	
Greenbelt	GGAO7108	GODZ	GR	33.23
Matera	MATERA	MATE	GR	58.00
Medicina	MEDICINA	MEDI	G	62.77
Metsahovi	METSAHOV	METS	G	128.88
Noto	NOTO	NOT1	G	71.69
Ny Ålesund	NYALES20	NYAL	G	112.44
Onsala	ONSALA60	ONSA	GR	79.57
Svetloe	SVETLOE	SVTL	GR	77.53
Westford	WESTFORD	WES2	GR	57.70
Wettzell	WETTZELL	WTZR	GR	139.45
Yebes	YEBES	YEBE	G	183.53

Table 3 Selected baselines; NS = north-south, EW = east-west, sys = GNSS with GPS (G), GLONASS (R)

Station 1	Station 2	Length [km]	Orientation	Sys
ONSA	WTZR	919.7	NS	GR
MATE	YEBE	1667.6	EW	G
MATE	ONSA	1891.1	NS	GR
GODZ	YEBE	5892.5	EW	G

3.2 Analysis of double-difference residuals

First, double-difference residuals $\hat{I}_{rs}^{ij}$ converted to L_1 will be analyzed. As mentioned above these residuals might be affected by float ambiguities. In accordance with the double-difference definition model-based ionospheric delays $\overline{I}_{rs}^{ij}$, biased by model accuracy and smoothing effects, can be computed. Besides these effects the differences $\hat{I}_{rs}^{ij} - \overline{I}_{rs}^{ij}$ are a first quality indicator. As individual differences might be strongly affected by unresolved ambiguities or model smoothing (e. g. during periods of higher ionospheric variability) our analysis is based on mean values and their standard deviation. For the following analysis the four baselines listed in Table 3 were selected. Figure 5 shows daily statistics for these baselines for 2013. The baseline lengths and the number of observed GNSS define the total number of double-differences formed for each baseline and day. The daily mean values are expected to be rather small as they represent the difference of four individual delays. For long baselines the large range of ionospheric conditions and the small number of commonly visible satellites will cause offsets and higher day-to-day variations. These effects are clearly visible in Fig. 5, where the baseline length has the greatest impact. However, by comparing the shorter east–west baseline MATE-YEBE (length 1667.6 km) against the north–south baseline MATE-ONSA (length 1891.1 km), also the major role of the baseline orientation becomes visible. When we consider the impact of baseline orientations the ionospheric variations with respect to both, latitude and time have to be discussed. Concerning latitudinal variations the ionosphere is divided into three regions: equatorial (below 30°), mid latitude and high latitude (above 60°).[3] As the baselines are located in the more quiet mid- and high-latitude regions the impact of latitudinal variations might be comparatively small. Time-dependent ionospheric density changes are strongly related to local time. East–west baselines will be highly affected by these variations as the local time will differ by several hours (e.g. $\Delta \mathrm{UT}_{\mathrm{GODZ-YEBE}} \approx 5\,\mathrm{h}$). Depending on solar activity and seasonal effects, changes in the total electron content of more than 10 TECU/h are possible (Zolesi and Cander 2013). The daily standard deviations are affected in the same way. Looking at the TEC values in Fig. 1 we see that higher standard deviations coincide with higher TEC values. When analyzing the discrepancies between the mean values as derived from residuals and from the models, even for GODZ-YEBE the differences are below 0.5 m. In general, therefore, a good agreement can be observed. Looking at the standard deviations for Onsala–Wettzell smaller values for $\overline{I}_{rs}^{ij}$ are visible. They might be caused by a smaller influence of the smoothed model related to the short baseline and the high number of double-differences. For the longer baselines the smoothing causes higher standard deviations for $\overline{I}_{rs}^{ij}$.

[3] With respect to a magnetic reference frame (latitude of the geomagnetic north pole is 87.2° N).

3.3 Analysis of single-difference delay corrections

The quality evaluation concerning the residual splitting is presented in two steps. First, epoch-wise standard deviations of delay corrections $\hat{I}_{rs}^{i}$ are computed to assess the impact of the number of visible satellites. The different zenith distances cause the major deviations between individual delays. To convert the original slant delay $\hat{I}_s$ to a vertical delay $\hat{I}_v$ the approximation

$$\hat{I}_v = \hat{I}_s \cdot \cos\left(\frac{R_E}{R_E + H} \cdot \sin\left(\frac{z_r + z_s}{2}\right)\right), \tag{9}$$

with the Earth's radius R_E, the ionospheric layer height $H = 350\,\mathrm{km}$ and the zenith distance z, was used. To compute the vertical delays for the corrections, formally the average zenith distance in Eq. 9 needs a compensation term (Wang et al. 2014). However, that term will not affect the characterization within this section. Figure 6 shows the standard deviation for all epochs as a function of the number of satellites. In order to include also a very short baseline we replaced the baseline MATE-ONSA by METS-SVTL (GPS, baseline length 298 km). In general, and in accordance with Fig. 5, the standard deviation is increasing with the baseline length. The increase with the number of satellites reflects that, especially for longer baselines, the better hemispheric coverage leads to larger differences in the delay corrections. The number of epochs with a certain number of satellites heavily depends on the baseline geometry and available GNSS as shown in the histogram in Fig. 6 (*right*).

Ideally the differences between slant ionospheric delays of consecutive epochs are given by ionosphere variations and the changed satellite position with respect to the baseline, i.e. in general they will be very small. If the zero-mean condition is applied for each epoch individually, all changes in the visible GNSS satellite constellation will cause additional variations in the derived ionospheric delays. Figure 7 shows the effect on the delays by computing the delay difference between consecutive epochs for the same satellite. Plotting these values as a function of mean zenith distance $\overline{z_m}$ defined

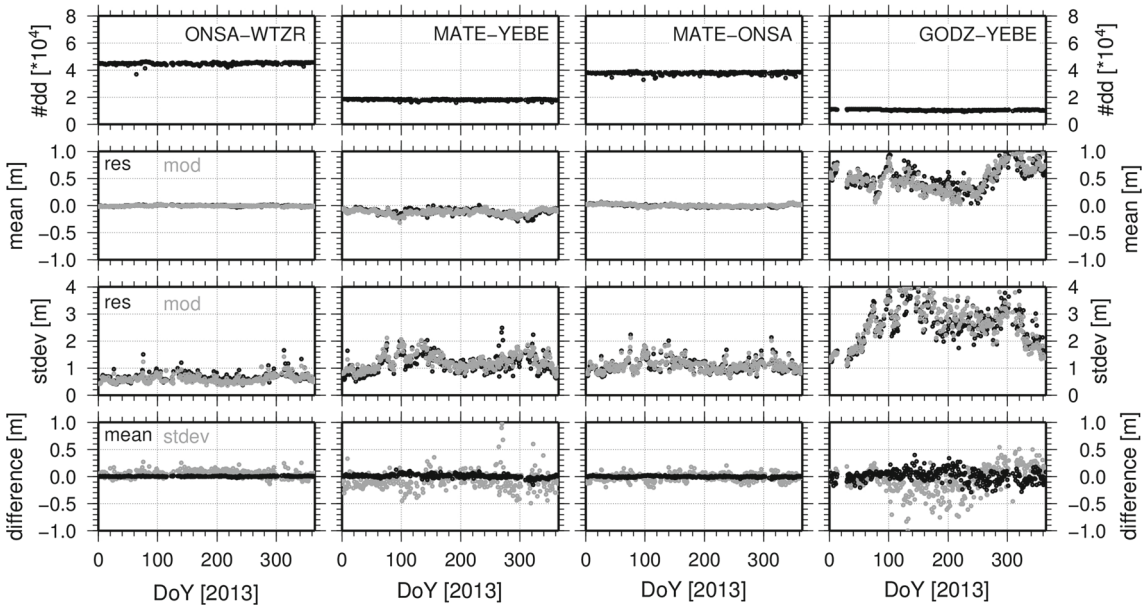

Fig. 5 Analysis of double differences; *first row* number of double differences (dd) per day, *second row* daily mean of $\hat{I}^{ij}_{rs}$ (*black*) and $\overline{I}^{ij}_{rs}$ (*gray*), *third row* daily standard deviation of $\hat{I}^{ij}_{rs}$ (*black*) and $\overline{I}^{ij}_{rs}$ (*gray*) and *forth row* difference of mean and standard deviation ($\hat{I}^{ij}_{rs} - \overline{I}^{ij}_{rs}$)

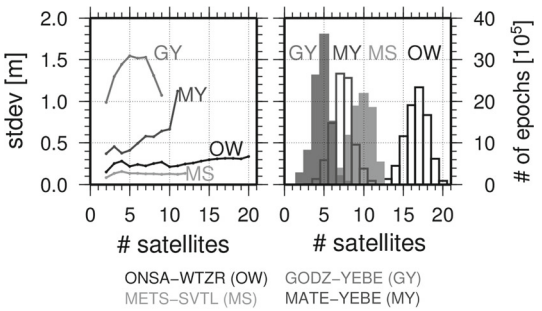

Fig. 6 Mean value of the epoch-wise standard deviation of the corrections *left* and the number of observed satellites per epoch (*right*)

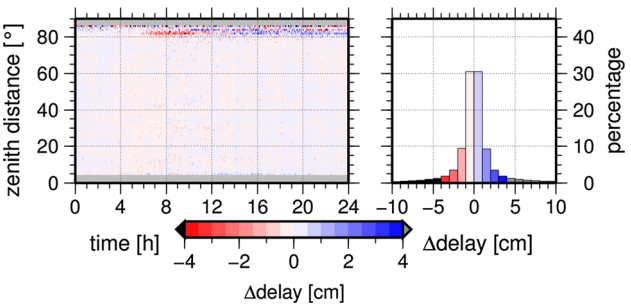

Fig. 7 Difference between delay corrections of consecutive epochs for baseline ONSA-WTZR and all days of 2013; *left* as a function of mean zenith distance and observation epoch and *right* as a histogram

by

$$\overline{z_m} = \frac{1}{2}\left(\frac{z^i(t_1) + z^j(t_1)}{2} + \frac{z^i(t_2) + z^j(t_2)}{2}\right) \tag{10}$$

and of the time of the day, in bins of 20 min and 2°, respectively, differences below 2 cm predominate. As the difference is computed by $\hat{I}^i_{rs}(t_1) - \hat{I}^i_{rs}(t_0)$ increasing delays are characterized by positive and decreasing delays by negative values. However, the deviations of single-difference corrections will only represent the differences not the ionospheric delays itself. Considering all differences, only a minor number exceeds 5 cm. This is visible in the histogram (Fig. 7, *right*), where 93.1 % of all computed differences are below 5 cm. Therefore, introducing the zero-mean constraints epoch-wise does not degrade the derived ionospheric delays.

3.4 Analysis of zero-difference residuals

The splitting of the single-difference residuals into zero-differences allows the analysis of station-specific effects. Using the delay differences between consecutive epochs as a quality criterion, the percentage of differences below 5 cm is 79 % for Wettzell. The biggest differences occur at low elevations showing decreasing values during day and increasing values during evening hours. In summary also the second splitting procedure does not significantly degrade the derived ionospheric delays.

Daily mean and monthly median values of the vertical delays for the IGS stations NOT1, WTZR and NYAL are plotted in Fig. 8. The main difference is caused by the station latitude: NOT1 and WTZR are located in the mid-latitude region, NYAL already in the high-latitude region. Seasonal effects are visible: one maximum occurs in spring (April, May and June) and a second one in autumn (October and

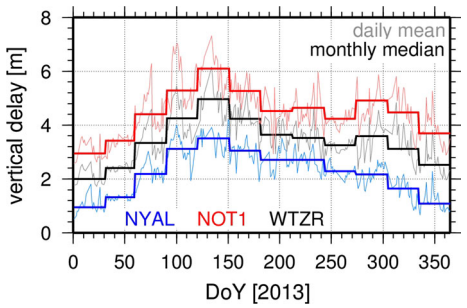

Fig. 8 Daily mean vertical delays and their monthly median value for stations NOT1 (36.8° N), WTZR (49.1° N) and NYAL (73.3° N)

November, not visible for NYAL). Decreasing day-to-day variations indicated by daily mean values can be found for higher station latitudes. More details concerning the variability of the free electron content and the ionospheric delay can be found, e.g., in Hernández-Pajares et al. (2009).

4 Validation using GNSS signals

For a first validation of the L4R corrections GNSS measurements will be used. When processing dual-frequency GNSS data by forming the ionospheric-free linear combination L_3, 99.9 % of the ionospheric delay for GNSS observations can be removed (Hernández-Pajares et al. 2011). The correction of remaining higher-order ionospheric effects is described, e.g., in Fritsche et al. (2005). The results of an L_3 processing (hereafter referred as V_{L3}) are assumed as "truth". Comparing them to single-frequency results, where the L4R delay corrections are applied (V_{L4R}), allows a quality assessment and validation of L4R. In addition, a comparison to solutions where only corrections derived from the CODE GIMs were applied (V_M) are possible. In the following, remaining residuals and station coordinate repeatabilites are studied corresponding to the processing scheme of Fig. 4.

To minimize the absorption of the ionospheric delay, while analyzing the residuals, all parameters except remaining ambiguities were fixed to their a-priori values. In a second step, station coordinates were estimated and their repeatabilities (i.e. the variation of daily solutions with respect to the combined solution) were studied.

4.1 Analysis of residuals

Figure 9 shows daily RMS values of remaining residuals for the 990 km long baseline Matera–Wettzell. The corresponding mean values are listed in Table 4. The receivers at Matera are denoted by MATE (MT) and MAT1 (0A), those at Wettzell by WTZR (WR) and WTZZ (0M). The RMS of V_{L3} is around 2 cm for both, a combined GPS/GLONASS and a GPS-only solution. Using the L4R delays to correct an GPS L_1 solution, the RMS increases slightly to 2.5 cm. Caused by a higher number of float ambiguities degrading the L4R corrections, the RMS of the combined solution increases to 4 cm, which is still rather small compared to V_M. However, the residuals highly benefit from introducing delay corrections derived from the same baseline, as in this case receiver noise, multipath and float ambiguities are identical. As Matera and Wettzell are equipped with more than one GPS receiver, a co-located baseline can be used to estimate the delay corrections and to assess the impact of different ambiguity, noise and multipath characteristics. The daily RMS values increase to 20–50 cm when applying delay corrections derived for the co-located baseline, although the RMS values are mainly below the V_M solution. Here the residuals are affected by a number of unresolved phase ambiguities in both baselines. However, this validation step cannot account for radio telescope biases and ambiguity-free delays in the real G-VLBI case. The G-VLBI residuals and results will also be limited by uncorrected biases in the radio telescope.

Analyzing other baselines with comparable lengths, e.g. Onsala–Wettzell and Matera–Onsala, the same level of RMS values can be obtained (Table 4). Comparing the RMS values for very long baselines, e.g. Wettzell–Greenbelt (GODZ, GODN), the V_{L3} RMS values are around 2.5 cm and increase to 8 cm for V_{L4R}, while V_M leads to RMS values >50 cm

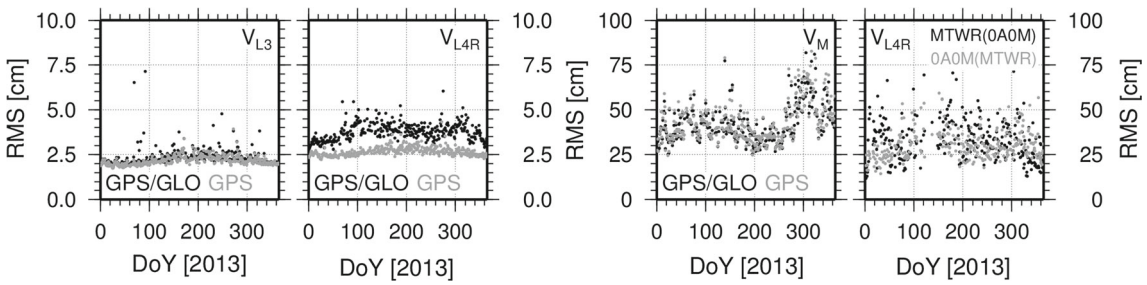

Fig. 9 Daily RMS of residuals for baseline Matera–Wettzell; *left* residuals of V_{L3} and residuals of V_{L4R}; *right* residuals of V_M and residuals of V_{L4R} (corrections derived by co-located baselines); plot 1-3: GPS/GLONASS (*black dots*) and GPS-only (*gray dots*), for plot 4 the *colors* identify two different baselines

Table 4 RMS statistics for baseline Matera–Wettzell (mean values and standard deviation [cm]); G = GPS, R = GLONASS; MT = MATE, 0A = MAT1, WR = WTZR, 0M = WTZZ

Baseline	L4R	Sys	V_{L3}	V_{L4R}	V_M
MTWR	MTWR	GR	2.33	3.77	42.33
			±0.50	±0.49	±11.01
MTWR	MTWR	G	2.18	2.66	43.56
			±0.26	±0.24	±12.29
0A0M	MTWR	G	2.35	30.20	43.63
			±0.20	±8.12	±13.17
MTWR	0A0M	G	2.18	33.39	43.56
			±0.21	±12.82	±12.78

Table 5 RMS statistics for baseline Greenbelt–Wettzell (mean values and standard deviation [cm]); G = GPS, R = GLONASS; GODZ = 05, GODN = G5, WR = WTZR, 0M = WTZZ

Baseline	L4R	Sys	V_{L3}	V_{L4R}	V_M
05WR	05WR	GR	2.52	7.83	53.39
			±0.27	±1.76	±10.36
G50M	G50M	G	2.46	7.50	54.34
			±0.37	±1.81	±10.82

(see Table 5). Residuals express the remaining errors, i.e. the remaining ionospheric delays and the effect of unresolved ambiguities, but not the impact on requested parameters. Therefore, a closer look at station coordinates and their repeatabilities is given in the next section.

4.2 Analysis of station coordinate repeatabilities

Station coordinates can be a major result for upcoming G-VLBI analyses. Therefore, the behavior of station coordinate repeatabilities was tested for the baselines Onsala–Wettzell, Onsala–Matera and Matera–Wettzell. The corresponding RMS values in north, east and up direction are listed in Table 6. The repeatablities are computed baseline-wise with keeping one station fixed. Considering the baseline length (third column of Table 6) there is a corresponding increase of the coordinate repeatabilities derived by V_{L4R} compared to V_{L3}. Nevertheless, the 1-cm coordinate repeatability is achieved for the first three baselines. Having a closer look at the height component of Matera–Wettzell (Fig. 10), no significant discrepancies between the results for the baselines MTWR and 0A0M are visible for solution types V_{L3} and V_M. In V_M, model deficiencies cause a higher noise level and higher day-to-day variations of the coordinate repeatabilities. They are at the level of a few dm. As the V_{L4R} coordinates of MTWR agree quite well, the impact of transferring corrections to an other baseline is investigated using the co-located baseline

Table 6 Coordinate repeatabilities in North, East and Up [cm]; M T= MATE, 0A = MAT1, ON = ONSA, WR = WTZR, 0M = WTZZ; baseline length is given in km

Baseline	L4R	(km)		V_{L3}	V_{L4R}	V_M
ONWR	ONWR	920	N	0.28	0.34	8.73
			E	0.19	0.29	3.29
			U	0.51	0.65	10.91
MTWR	MTWR	990	N	0.23	0.32	9.39
			E	0.17	0.35	4.23
			U	0.29	0.54	15.38
MTON	MTON	1890	N	0.30	0.44	7.62
			E	0.27	0.57	4.16
			U	0.34	0.89	15.20
0A0M	MTWR	990	N	0.31	3.74	9.63
			E	0.18	2.41	4.85
			U	0.28	3.83	15.96

0A0M. As a consequence, the repeatabilities increase to a level of a few cm and show higher day-to-day variations. This degradation might again be mainly caused by float ambiguities in both baselines.

In Fig. 11 (left) coordinate repeatabilities for all baselines containing Wettzell are shown. In the case of using the same baseline to derive L4R corrections V_{L4R} is clearly superior to V_M. Except for the longer baselines between Westford and Wettzell resp. Greenbelt and Wettzell, V_{L4R} is nearly as good as V_{L3}. Unfortunately, only a small number of the selected sites are equipped with more than one GNSS receiver delivering to the IGS. Therefore, we modified the co-located baseline comparison in such a way that one station is identical for the estimation of L4R corrections and the L_1 processing. In the following we replaced WTZR by WTZZ in the L_1 processing part. As visible in Fig. 11 (right) the repeatabilities increase with the baseline length. For the long baselines V_M gives the better results. This is a consequence of the lower percentage of resolved ambiguities in L4R.

5 Validation using VLBI signals

The second validation part aims at getting closer to the G-VLBI situation shown in Fig. 2. Therefore, the ionospheric delays derived with the L4R approach are validated against ionospheric delays estimated from dual-frequency VLBI observations to quasars. In order to compare identical ionospheric situations, requirements concerning the spherical distance α_j between the satellite and the quasar observed at epochs t_j^i and t_j^q, respectively, have to be fulfilled for both stations $j = (1, 2)$ of the VLBI baseline:

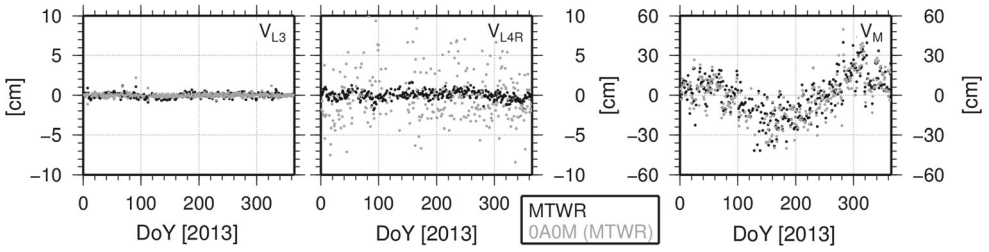

Fig. 10 Daily height coordinate repeatability for Matera–Wettzell; *left* V_{L3} and V_{L4R}; *right* V_M; repeatabilities for MTWR (*black dots*) and 0A0M with L4R corrections derived from MTWR (*gray dots*)

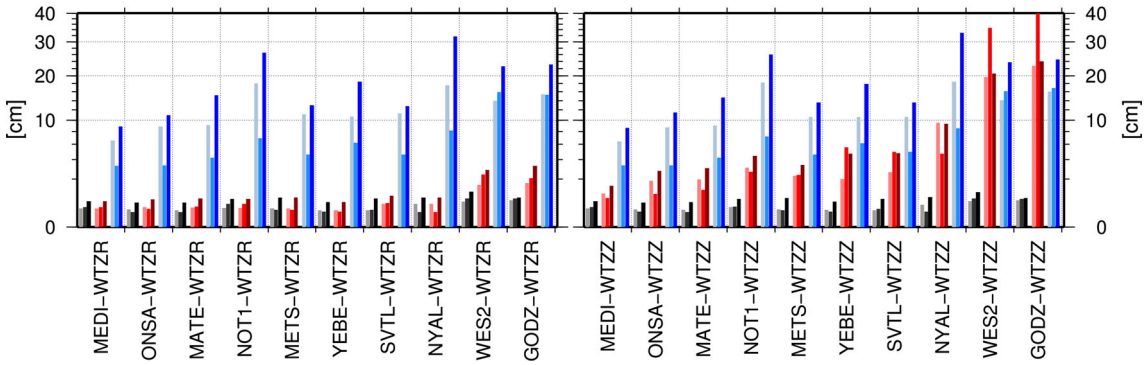

Fig. 11 Coordinate repeatabilities for V_{L3} (*black*), V_{L4R} (*red*) and V_M (*blue*); *left* same baseline for L4R and processing; *right* co-located baseline for the processing; each triplet shows the north, east and height component; the baselines are sorted regarding their baseline length

$$\alpha_1 < 3^\circ \text{ and } \alpha_2 < 3^\circ \tag{11}$$

$$\Delta t_1 < 15' \text{ and } \Delta t_2 < 15' \text{ with } \Delta t_j = t_j^i - t_j^q. \tag{12}$$

The spherical distance α_j for each station is computed by

$$\alpha_j = \cos^{-1}\left(\sin(\epsilon_j^i)\sin(\epsilon_j^q) + \cos(\epsilon_j^i)\cos(\epsilon_j^q)\cos(\Delta a_j)\right)$$

$$\text{with } \Delta a_j = \frac{a_j^q - a_j^i}{\cos\left(\frac{\epsilon_j^i + \epsilon_j^q}{2}\right)}, \tag{13}$$

where ϵ_j^i, ϵ_j^q denote the elevation angle of the satellite and quasar, respectively, and a_j^i, a_j^q the corresponding azimuth angles. GNSS observations who meet these conditions will be called *associated observations*. The ionospheric delays for VLBI are computed using the X-band and S-band observations provided via the NGS Card observation files;[4] in the following they are referred to as NDC (**N**GS **d**elay **c**orrection). In the next session these delays will be discussed in more detail. As the correction values computed by L4R are provided in TECU, also the NDC values are converted to TECU using Eq. 3. The validation results are finally reconverted into metric units using the VLBI X-band frequency.

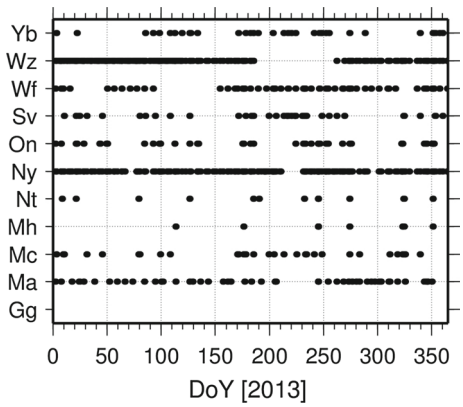

Fig. 12 Availability of VLBI observations during 2013; *each dot* indicates that the corresponding station was part of the VLBI network

5.1 VLBI database and theoretical considerations

Together with the GNSS data the above-described quasar observations from different VLBI sessions in 2013 were used. According to the DBC-codes described by the IVS master file format description[5] XA, XB, XE, XH and XK sessions were analyzed. Figure 12 shows the participation of each radio telescope (see also Table 2) within the analyzed VLBI sessions. Station GGAO7108 at Greenbelt, MD, USA was chosen, but participated only in the skipped intensive ses-

[4] http://lacerta.gsfc.nasa.gov/mk5/help/dbngs_format.txt, Oct 2014.

[5] ftp://ivscc.gsfc.nasa.gov/pub/control/master-format.txt, Oct 2014.

sions. By using the remaining 10 VLBI stations, 45 baselines could be defined with lengths between 200 and 7200 km. The following steps were carried out in a baseline-wise mode.

Considering the threshold value for the direction difference, comparable to the separation angle γ, the maximally possible baseline length $b_{\max}$ can be calculated by

$$b_{\max} = 2R \sin^{-1}\left(a_{\mathrm{GNSS}} \frac{\sin\gamma}{R_E}\right). \tag{14}$$

Depending on the semi-major axis a_{GNSS} of the GNSS considered and testing the conditions (Eq. 11) individually, the maximal baseline length for $\alpha_j = 3°$ results in 2796 km (2690 km for GLONASS); hence 28 out of the 45 baselines theoretically available can be used. Assessing the possible total area of the hemisphere covered by these requirements gives the probability of finding associated observations. Using the given threshold values approx. 5 % (GPS and GLONASS) of the hemisphere is covered. Therefore, the number of usable quasars will be rather small. Considering the different ionospheric conditions acting on the signals separated by $\alpha = 3°$ the horizontal distance between the ray paths can be computed. For zenith distances of 10° the distance is below 50 km also at a height of 1000 km, for elevations below 5° the separation at an altitude of 1000 km will be larger than 300 km, obviously leading to distinct TEC differences. Concerning the VLBI ionospheric delays two effects are worth mentioning. First, the ionospheric signals derived by X/S-band signals of quasars are also affected by the interplanetary and interstellar plasma. Sekido et al. (2003) assumed that the additional delay is below one TECU. Second, the VLBI ionospheric delays $\tau'_{X,ion}$, that are derived directly from the differences between the X- and S-band observations as defined by Hobiger (2006), contain the instrument-specific offsets $\tau_{1,\mathrm{inst}}$ and $\tau_{2,\mathrm{inst}}$:

$$\tau'_{X,\mathrm{ion}} = \frac{f_S^2}{f_X^2 - f_S^2}(\tau_X - \tau_S) + \tau_{1,\mathrm{inst}} - \tau_{2,\mathrm{inst}}. \tag{15}$$

These instrument-specific offsets are typically absorbed by the receiver clock estimation and can be considered as constant during one session (Sekido et al. 2003). This allows to study the difference of the ionospheric delays derived by GNSS and VLBI without knowing $\tau_{1,inst}$, $\tau_{2,inst}$ by either analyzing the differences after subtracting the session-wise mean value or by analyzing the session-wise standard deviation (only if more than 10 associated observations for one session are available).

5.2 Validation results for single-difference L4R corrections

In a first step, differences NDC-L4R were computed for all associated observations by subtracting the corresponding mean difference. Figure 13 (*right*) shows these reduced differences in a histogram: 91 % of these differences are below 5 cm. In Fig. 13 (*left* and *center*) the reduced differences are plotted as a function of their observation time and the mean of both quasar elevations. In the first case only small systematic effects are visible. Concerning the elevation, caused by the observation geometry, the number of associated observations is decreasing with increasing elevation angle. Due to the longer signal paths within the ionosphere and larger distances between the signal paths, differences increase for low elevations.

Figure 14 shows the number of associated observations for each session and baseline together with the derived standard deviation for the single-difference case (*black dots*). In total, 3014 associated observations for 66 baseline-session pairs were analyzed; 96 % of them show a standard deviation smaller than 5 cm. The mean of 1.6 cm and the median of 1.4 cm (corresponding to 2.7 and 2.2 TECU) are quite small. Because of the baseline geometry and the GNSS satellite trajectories only five out of the 28 possible baselines contribute a significant number of associated observations. In view of the definition of associated observations it is clear that the standard deviations also contain effects caused by the distribution across the hemisphere and the distribution over time. Also the variable ionospheric behavior within the window in direction and time has an impact on the delay differences. This is discussed in Sect. 5.4.

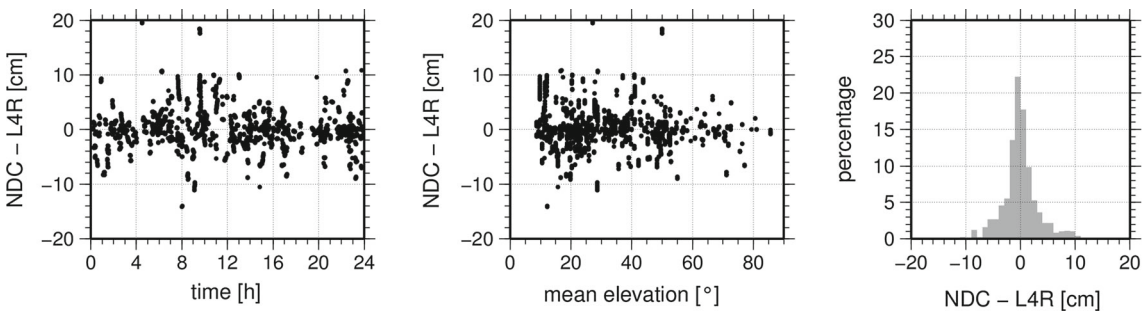

Fig. 13 Differences NDC-L4R (after subtracting a session-specific mean value) for single-difference L4R corrections with respect to observation time (*left*), mean quasar elevation (*middle*) and as a histogram (*right*)

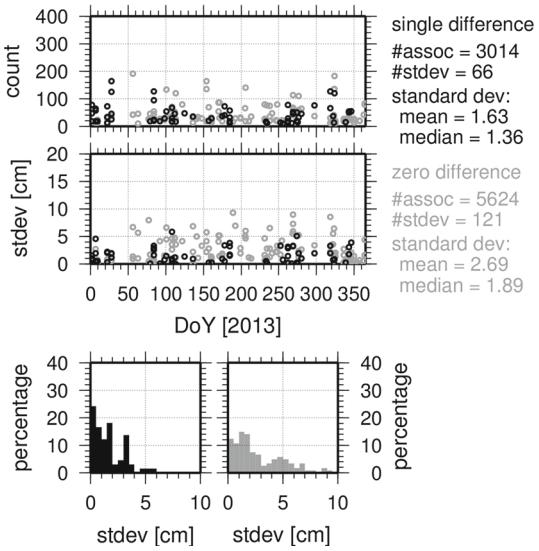

Fig. 14 Statistics for the validation using VLBI observations: number of associated observations for all baselines and sessions (*top*), corresponding standard deviations (*middle*) and a histogram of the standard deviations (*bottom*); L4R corrections based on single-differences (*black*) and zero-differences (*gray*)

5.3 Validation of zero-difference corrections

If the ionospheric corrections are derived for zero differences, two different GNSS satellites or one satellite at different epochs t_1^i, t_2^i might be used for validation, too. Depending on the time difference $t_1^1 - t_2^1$ and the elevation difference distinct variations of the ionospheric delays are possible. In order to avoid large degradation in the derived corrections, the time difference $\Delta t = t_1^1 - t_2^1$ has been limited to 30 seconds. In fact, the number of associated observations increases dramatically compared to the single-difference case, if different observation epochs for one GNSS satellite within the time threshold (Eq. 12) are allowed. Figure 14 shows this increase for the zero-difference L4R corrections (*gray dots*). The standard deviations show no significant systematic difference. Also here the majority (around 85 %) of all standard deviations, estimated baseline- and session-wise, are below 5 cm.

In the zero-difference validation 14 out of 28 baselines contribute a significant number of associated observations. The increasing in the standard deviations compared to the single-difference case are due to the involvement of two different GNSS satellites in combination with a minor degradation of the ionospheric corrections derived from zero-differences due to the second splitting procedure.

5.4 Impact of threshold values

In Sect. 5.1 the total area of the hemisphere covered by the available set of GNSS satellites was shortly addressed. In fact, for this validation type, the balance between wide open and very restrictive threshold values is crucial. Using very restrictive conditions for associated observations (reducing degrading effects caused by different signal paths) will lead to a small, probably too low data amount. On the other side, using data too far away from the VLBI observation and the original ionospheric situation will also degrade the results. This is shown in Fig. 15 for each of the requirements by fixing the other conditions and using single-difference L4R corrections. Naturally both, the mean number of associated observations per session and the corresponding standard deviations, are increasing when threshold values increase. A limitation on the spherical distance between satellite and quasar has a bigger impact than the time offset. Also the number of observations increases quite slowly while increasing the time window. In summary, the chosen threshold values allow a good balance between the number of associated observations and assuring the same ionospheric conditions as shown by the 40 observations per session and the standard deviations below 2 cm.

6 Conclusions and outlook

G-VLBI observations will be a great opportunity for the integration of VLBI into the co-location of geodetic space techniques in space. Correcting for the ionospheric delays will be mandatory, as G-VLBI observations might be single-frequency data. Using GNSS phase observations derived

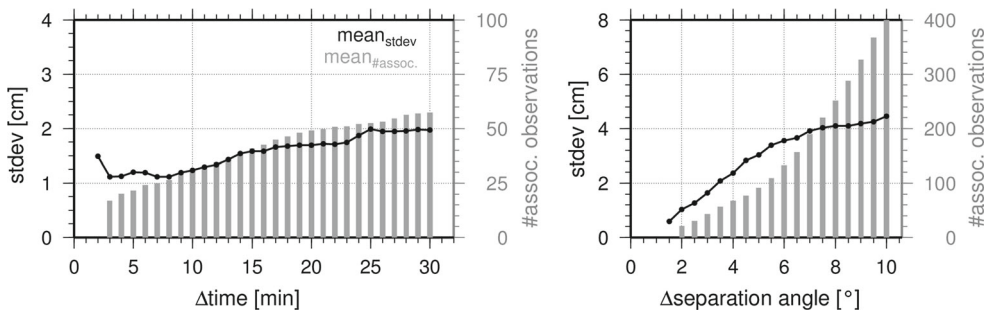

Fig. 15 Effect of the chosen threshold values for time and separation angle: the mean value of the corresponding number of associated observations (*gray bars*) and the overall mean value of the standard deviations for all available baselines (*black line*)

from co-located GNSS receivers by the L4R method is a good possibility to compute corresponding corrections. Other approaches to correct the ionospheric delays might result in a lower accuracy or enforce a different observation concept. The range of L4R applications is, in principle, limited to the tracking of GNSS satellites, as the main advantage consists in the observation of the same L-band signal. However, in special cases the L4R method might be suitable for single-frequency astrometry.

The validation of the L4R approach presented here using the geometry-free linear combination shows good results especially for the baselines between radio telescopes already used for G-VLBI (Onsala, Wettzell, Medicina). A 1-cm daily repeatability level for baseline coordinates could be achieved when introducing the L4R corrections into an L_1-based coordinate estimation. Differences to ionospheric delays from VLBI also show a good agreement at the level of a few TECU. For longer baselines, the method could not be tested against VLBI ionospheric delays as the quasar and the satellite could not be observed from both stations at roughly the same time. However, for such baselines a precise point processing (PPP) including ambiguity resolution might be preferable, as the double-difference approach suffers from the small number of common satellites. One opportunity for improvement will be the introduction of ionospheric models with higher spatial and temporal resolution. In the future, L4R will be tested using the first real G-VLBI observations available. The results will not only show the potential of these observations but also the potential of our method for correcting the ionospheric delays.

Acknowledgments The authors want to thank IVS and IGS for providing the necessary observations and CODE and TU Vienna for providing GNSS and atmospheric products allowing a suitable processing. They would also like to thank three anonymous reviewers for their assistance in evaluating this paper and their helpful recommendations. This work was done within the project "Co-location of Space Geodetic Techniques on Ground and in Space" which is part of the DFG funded Research Unit "Space-Time Reference Systems for Monitoring Global Change and for Precise Navigation in Space" (FOR 1503).

References

Alber C, Ware R, Rocken C, Braun J (2000) Obtaining single path phase delays from GPS double differences. Geophys Res Lett 27:2661–2664. doi:10.1029/2000GL011525

Altamini Z, Collilieux X, Métivier L (2011) ITRF2008: an improved solution of the international terrestrial reference frame. J Geod 85:457–473. doi:10.1007/s00190-011-0444-4

Bar-Sever YE, Haines B, Wu S, Lemoine F, Willis P (2009) Geodetic reference antenna in space (GRASP): a mission to enhance the terrestrial reference frame. In: COSPAR colloquium: scientific and fundamental aspects of the Galileo program, Padua

Beutler G, Baueršíma I, Gurtner W, Rothacher M, Schildknecht T, Geiger A (1988). Atmospheric refraction and other important biases in GPS carrier phase observations. In: Atmospheric effects on geodetic space measurements, monograph 12. School of Surveying, University of New South Wales, Kensington, pp 15–43

Böhm J, Werl B, Schuh H (2006) Troposphere mapping functions for GPS and VLBI from European Centre for medium-range weather forecasts operational analysis data. J Geophy Res 111(B2). doi:10.1029/2005JB003629

Corey B (2001) IVS/IGS/ILRS Working Group on GPS phase center mapping. In; Vandenberg NR, Baver KD (eds) International VLBI service for geodesy and astrometry 2000 annual report. NASA/TP-2001-209979

Crocetto N, Pingue F, Ponte S, Pugliano G, Sepe V (2008) Ionospheric error analysis in GPS measurements. Ann Geophys 51(4):585–595. doi:10.4401/ag-4456

Dach R (2013) Bernese GNSS software: new features in version 5.2. Astronomical Institute, University of Bern, Switzerland

Dach R, Hugentobler U, Fridez P, Meindl M (2007) Bernese GPS software version 5.0. Astronomical Institute, University of Bern, vol 640, pp 114

Dickey JM (2010) How and why to do VLBI on GPS. In: Behrend D, Baver KD (eds) VLBI2010: from vision to reality, IVS 2010 general meeting Proceedings, NASA/CP2010215864. NASA, Goddard Space Flight Center

Duev DA, Calvés GM, Pogrebenko SV, Gurvits LI, Cimo G, Bahamon TB (2012) Spacecraft VLBI and Doppler tracking: algorithms and implementation. Astron Astrophys 541:A43. doi:10.1051/0004-6361/201218885

Flohrer C, Otten M, Springer T, Dow J (2011) Generating precise and homogeneous orbits for Jason-1 and Jason-2. Adv Space Res 48:152–172. doi:10.1016/j.asr.2011.02.017

Fritsche M, Dietrich R, Knöfel C, Rülke A, Vey S, Rothacher M, Steigenberger P (2005) Impact of higher-order ionospheric terms on GPS estimates. Geophy Res Lett 32. doi:10.1029/2005GL024342

Gordon D (2010) Use of GPS TEC maps for calibrating single band VLBI sessions. In: Behrend D, Baver KD (eds) VLBI2010: from vision to reality, IVS 2010 general meeting Proceedings, NASA/CP2010215864. NASA, Goddard Space Flight Center, pp 242–246

Hase H (1999) Phase centre determinations at GPS-satellites with VLBI. In: Proceedings of the 13th working meeting on European VLBI for geodesy and astrometry

Haas R, Neidhardt A, Kodet J, Plötz C, Schreiber U, Kronschnabl G, Pogrobenko S, Duev D, Casey S, Martl-Vidal I, Yang J, Plank L (2014) The Wettzell-Onsala G130128 experiment—VLBI observation of a GLONASS satellite. In: Behrend D, Baver K, Armstrong K (eds) IVS 2014 general meeting Proceedings. Science Press

Hawarey M, Hobiger T, Schuh H (2005) Effects of the 2nd order ionospheric terms on VLBI measurements. Geophys Res Lett 32:L11304. doi:10.1029/2005GL022729

Hernández-Pajares M, Juan JM, Sanz J, Orús R, Garcia-Rigo A, Feltens J, Komjathy A, Schaer S, Krankowski A (2009) The IGS VTEC maps: a reliable source of ionospheric information since 1998. J Geod 83(3–4):263–275. doi:10.1007/s00190-008-0266-1

Hernández-Pajares M, Juan JM, Sanz J, Aragón-Àngel À, García-Rigo A, Salazar D, Escudero M (2011) The ionosphere: effects, GPS modeling and the benefits for space geodetic techniques. J Geod 85(12):887–907. doi:10.1007/s00190-011-0508-5

Hobiger T (2006) VLBI as a tool to probe the ionosphere. Ph.D. thesis, Institute of Geodesy and Geophysics, TU Vienna. ISSN: 1811-8380

Kikuchi F, Liu Q, Matsumoto K, Hanada H, Kawano N (2008) Simulation analysis of differential phase delay estimation by same beam VLBI method. Earth Planets Space 60(4):391–406

Kikuchi F, Liu Q, Hanada H, Kawano N, Matsumoto K, Iwata T, Goossens S, Asari K, Ishihara Y, Tsuruta S-I et al (2009) Picosecond accuracy VLBI of the two subsatellites of SELENE (KAGUYA) using multifrequency and same beam methods. Radio Sci 44(2). doi:10.1029/2008RS003997

Kodet J, Plötz USA, Neidhardt A, Kronschnabl G, Haas R, Calvès GM, Pogrebenko S, Rothacher M, Männel B, Plank L, Hellerschmied A (2014) Co-locations of space geodetic techniques on ground and in space. In: Behrend D, Baver K, Armstrong K (eds) IVS 2014 general meeting Proceedings. Science Press

Männel B, Rothacher M, Kodet J, Schreiber U, Schmid R (2014) GLONASS Satellites Simultaneously Observed by VLBI, GNSS and SLR. In: Behrend D, Baver K, Armstrong K (eds) IVS 2014 general meeting Proceedings. Science Press

Plank L (2013) VLBI satellite tracking for the realization of frame ties. Veröffentlichungen des Departments für Geodäsie und Geoinformation, Vienna University of Technology, Geowissenschaftliche Mitteilungen, p 95

Plank L, Böhm J, Schuh H (2014) Precise station positions from VLBI observations to satellites: a simulation study. J Geod 88:1–15. doi:10.1007/s00190-014-0712-1

Prölss G (2008) Ionospheric storms at mid-latitude: a short review. Mid-latid Ionos Dyn Disturb 181:9–24. doi:10.1029/181GM03

Sardon E, Rius A, Zarraoa N (1994) Estimation of the transmitter and receiver differential biases and the ionospheric total electron content from global positioning system observations. Radio Sci 29(3):577–586. doi:10.1029/94RS00449

Schaer S (1999) Mapping and predicting the Earth's ionosphere using the global positioning system. Ph.D. thesis, Universität Bern. ISBN: 3-908440-01-7

Schmid R (2009) Zur Kombination von GPS und VLBI. Ph.D. thesis, Technische Universität München

Sekido M, Kondo T, Kawai E (2003) Evaluation of GPS-based ionospheric TEC map by comparing with VLBI data. Radio Sci 38:1069. doi:10.1029/2000RS002620

Sovers OJ, Fanselow JL, Jacobs CS (1998) Astrometry and geodesy with radio interferometry: experiments, models, results. Rev Mod Phys 70:1393–1454. doi:10.1103/RevModPhys.70.1393

Steigenberger P, Rothacher M, Dietrich R, Fitsche M, Rülke A, Vey S (2006) Reprocessing of a global GPS network. J Geophy Res 113. doi:10.1029/2005JB003747

Thaller D, Dach R, Seitz M, Beutler G, Mareyen M, Richter B (2011) Combination of GNSS and SLR observations using satellite co-locations. J Geod 85(5):257–272. doi:10.1007/s00190-010-0433-z

Tierno Ros C, Böhm J, Schuh H (2011) Use of GNSS-derived TEC maps for VLBI observations. In: Proceedings of the 20th meeting of the European VLBI Group for Geodesy and Astrometry

Tornatore V, Haas R, Deev D, Pegrebenko S, Casey S, Calvés GM, Keimpema A (2011) Single baseline GLONASS observations with VLBI: data processing and first results. In: Proceedings of the 20th meeting of the European VLBI Group for Geodesy and Astrometry

Tornatore V, Haas R, Deev D, Pegrebenko S, Casey S, Calvés GM (2014) Direct VLBI observations of global navigation satellite system signals. In: Rizos C, Willis P (eds) Earth on the edge: science of a sustainable planet. doi:10.1007/978-3-642-37222-3_32

Wang K, Meindl M, Geiger A, Rothacher M, Scaramuzza M, Troller M, Truffer P (2014) Assessment of single-difference ionospheric residuals in a regional network for GBAS. In: Proceedings of the 27th international technical meeting of the satellite division of the Institute of Navigation (ION GNSS+ 2014), Tampa, pp 2384–2393

Zolesi B, Cander LR (2013) Ionospheric prediction and forecasting. Springer Geophysics, Springer, Berlin. doi:10.1007/978-3-642-38430-1